

Heralded state preparation in a superconducting qubit

J. E. Johnson,¹ C. Macklin,² D. H. Slichter,² R. Vijay,² E. B. Weingarten,¹ John Clarke,¹ and I. Siddiqi²

¹*Department of Physics, University of California, Berkeley, California 94720, USA*

²*Quantum Nanoelectronics Laboratory, Department of Physics,
University of California, Berkeley, California 94720, USA*

(Dated: February 27, 2012)

We demonstrate high-fidelity, quantum non-demolition, single shot readout of a superconducting flux qubit in which the pointer state histograms can be resolved to below one part in 1000. In the weak excitation regime, continuous measurement permits the use of heralding to ensure initialization to a fiducial state, such as the ground state. This procedure boosts readout fidelity to 93.9% by suppressing errors due to spurious thermal population. Heralding also enables a simple, fast qubit reset protocol without changing the system parameters to induce Purcell relaxation.

PACS numbers: 03.67.Lx, 42.50.Lc, 42.50.Pq, 85.25.-j

Recent progress in superconducting qubits [1–4] has resulted in coherence times exceeding $10\ \mu\text{s}$ [5, 6] as well as the demonstration of multi-qubit algorithms [7, 8], further validating superconducting circuits as a viable platform for quantum information processing. The simultaneous realization of a fast, high-fidelity, quantum non-demolition (QND) qubit readout, however, has thus far been difficult, with many schemes exhibiting either sub-unity visibility [9], long measurement times [10, 11], or demolition of the quantum state [12]. Low power dispersive readouts based on circuit quantum electrodynamics (cQED) [13, 14] have demonstrated QND operation [15] with near unity visibility, thus faithfully mapping the qubit state to distinct frequency shifts of a microwave resonator [16]. Traditionally, insufficient measurement sensitivity has limited the fidelity with which these pointer states can be resolved in this architecture. Recent advances in low-noise superconducting amplifiers have provided a sufficiently high signal-to-noise ratio (SNR) [17, 18] to resolve the state of the measurement cavity in a time much shorter than the qubit relaxation time T_1 , and thus achieve single-shot readout.

In this Letter, we use a high speed readout based on a Josephson parametric amplifier (paramp) [19] to insert an additional measurement pulse before a qubit manipulation and measurement sequence to verify that the quantum system is initialized in the ground state. Such heralding techniques are currently employed in other quantum information architectures, for example trapped ion [20] systems. With this technique, we effectively eliminate state preparation errors due to the spurious excited state population commonly observed in superconducting qubits [21]. Furthermore, this method permits a rapid, deterministic reset of the qubit state—a particularly important function in long-lived qubits where simply waiting for a time much longer than T_1 is impractical.

An overview of the qubit chip is shown in Fig. 1 (a). The flux qubit and quasi-lumped-element measurement resonator are fabricated from aluminum on a silicon substrate using double-angle shadow evaporation. The res-

onator is formed by the parallel combination of an interdigitated finger capacitor ($C_r = 600\ \text{fF}$) and meander line inductor ($L_r = 1.3\ \text{nH}$), providing a measured resonant frequency $\omega_r/2\pi = 5.780\ \text{GHz}$. The resonator is coupled to the $50\text{-}\Omega$ feed lines by planar coupling capacitors, which set the resonator linewidth $\kappa/2\pi = 9\ \text{MHz}$. A perforated metal plane surrounds the resonator and forms the ground reference for an on-chip, co-planar waveguide (CPW) input for both the qubit manipulation and readout pulses.

The three-junction flux qubit (loop dimensions $3.8 \times 4.0\ \mu\text{m}^2$) is inductively coupled to the resonator through a shared, $2.6\text{-}\mu\text{m}$ length of a 150-nm -wide constriction in the meander line inductor. The qubit is flux biased with a small superconducting coil mounted on the outside of the copper box containing the qubit chip. The cryopackage is anchored to the $30\ \text{mK}$ base temperature stage of a liquid-cryogen-free dilution refrigerator. A schematic of the cryogenic portion of the microwave measurement circuit is shown in Fig. 1 (b). Qubit control and readout pulses are injected through the weakly coupled port of a directional coupler. The readout pulse is reflected from the resonator, acquiring a qubit-state-dependent phase shift. The reflected pulse passes through a series of circulators and a second directional coupler to the paramp, where it is amplified and reflected to the output port. The readout signal is further amplified by cryogenic and room-temperature amplifiers before it is down-converted to zero frequency and digitized in 10-ns increments.

The paramp is flux biased to match the qubit readout frequency and operated in phase-sensitive mode, wherein a strong pump tone is applied at the same frequency as the readout pulse. In this operating mode the phase of the reflected pump depends very sensitively on its power. If a small input signal is added in phase with the pump signal, the resulting small change in net power leads to a large phase shift. This form of amplification theoretically adds no additional noise to the measurement, allowing the overall noise temperature of the system to remain close to the standard quantum

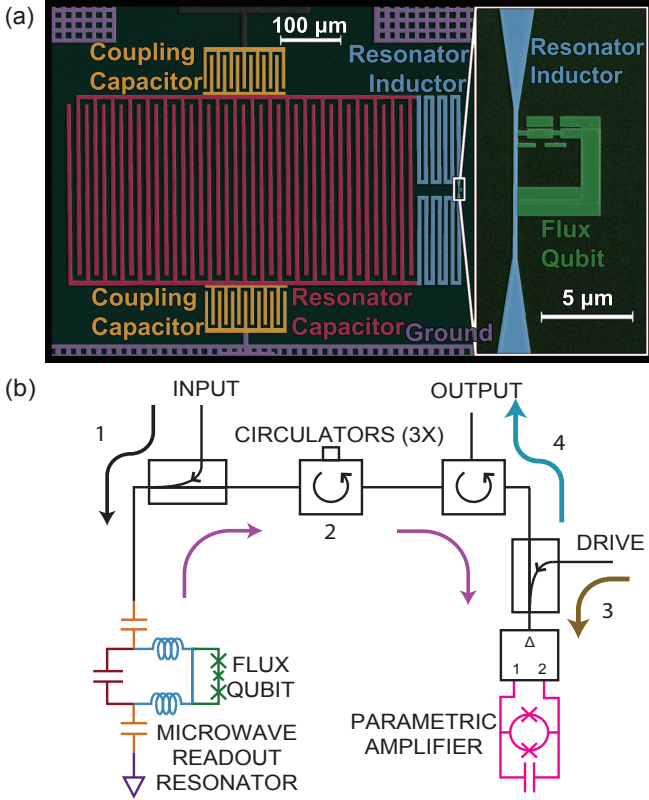


FIG. 1. Experimental setup. (Color online) (a) False color SEM image of the qubit and readout resonator with a magnified inset of the qubit. (b) Path of the readout signal at 30 mK.

limit $T_Q = \hbar\omega/2k_B = 139$ mK. Previous research has demonstrated noise temperatures close to this limit [19]. All measurements in the current work were made with the paramp providing 20-dB gain with an instantaneous bandwidth of 7 MHz.

We use spectroscopy to determine the flux qubit parameters $\Delta/\hbar = 6.15$ GHz (energy splitting at the degeneracy point) and $I_q = 204$ nA (circulating supercurrent in the qubit loop) [22]. The coupling strength between the qubit and resonator is $g/2\pi = 105$ MHz. In this geometry, the effective coupling strength is given by $g' = g \sin(\theta)$, where $\sin(\theta) = \Delta/\hbar\omega_{01}$; $\omega_{01}/2\pi$ is the qubit transition frequency. We extract the total qubit-resonator mutual inductance $M_t = g/I_q I_r = 6.3$ pH, where $I_r = \sqrt{\hbar\omega_r/L_r} = 54$ nA is the rms zero-point current in the resonator [23]. The qubit is flux biased away from the degeneracy point to $\omega_{01}/2\pi = 7.80$ GHz, corresponding to a detuning $\delta/2\pi = 2.02$ GHz. At this bias the dispersive shift is $2\chi/2\pi = 7.4$ MHz, producing a 150° phase shift between the two qubit pointer states. We measure a relaxation time $T_1 \approx 1.8$ μ s, achieved at the expense of a reduced $T_2^* = 55$ ns away from the flux-noise-protected degeneracy point.

We first determine the measurement SNR, in particu-

lar the degree to which we can separate the pointer state histograms. Our measurement protocol involves energizing the readout cavity with an average photon population \bar{n} . After 90 ns, when the cavity has essentially reached its steady state, we digitize the homodyne signal at 10^8 samples/s. Figure 2 (a) shows a portion of the readout signal as a function of time for three separate measurement traces at $\bar{n} = 14.6$ photons. The dashed line indicates the discrimination threshold voltage for associating the cavity response with the ground or excited state of the qubit. The system SNR is sufficiently high to enable single-shot discrimination of the readout pointer states in a single 10-ns integration bin. Quantum jumps from the excited to ground state of the qubit are observed as an abrupt downward jump in the signal. The characteristic decay time extracted from an exponential fit to the distribution of downward jump times agrees with the value of T_1 obtained from the ensemble averaged measurements.

In Fig. 2 (b), we present histograms as a log-linear plot of many ground and excited state preparations calculated immediately after the cavity has come to equilibrium. The presence of the smaller, secondary peak in each distribution indicates partial contamination of the pure states and leads to fidelity loss. The histograms are well separated but there is a small number of errant counts, that is, counts at values of the homodyne voltage not centered about the bimodal peaks. We attribute these counts to instances where a transition from one qubit state to the other occurs during the measurement. These transitions can be induced by noise or by T_1 relaxation.

We use these state histograms to calculate the readout fidelity $F = 1 - P_0 - P_1$ where P_0 and P_1 are the fraction of error counts observed for a fixed discrimination threshold voltage. The uncorrected readout fidelity as a function of readout power is presented in Fig. 3. The ‘10-ns’ fidelity series is calculated from the histograms of the homodyne voltage values from a single 10-ns digitization bin, as described above. The ‘integrated’ data series is calculated by integrating the entire readout signal weighted with an exponentially decaying filter [24]. The optimal filter time constant is empirically determined for each readout power to maximize the fidelity. At very low power, the ‘10-ns’ fidelity is severely suppressed because the system SNR is low. A substantial fraction of the lost fidelity can be recovered through integration. As expected, fidelity increases with increasing readout power and the two methods produce identical results above $\bar{n} \approx 10$, where the ‘10-ns’ readout histograms become well-separated. The highest measured fidelity is $91.1 \pm 0.4\%$ at $\bar{n} = 37.8$. In Fig. 3 we also plot the qubit relaxation time T_1 of the ensemble averaged signal during readout after an excited state preparation. As the power is further increased above $\bar{n} = 100$, the fidelity and T_1 both decrease as a result of increasing readout backaction. Below $\bar{n} = 14.6$, T_1 during readout always

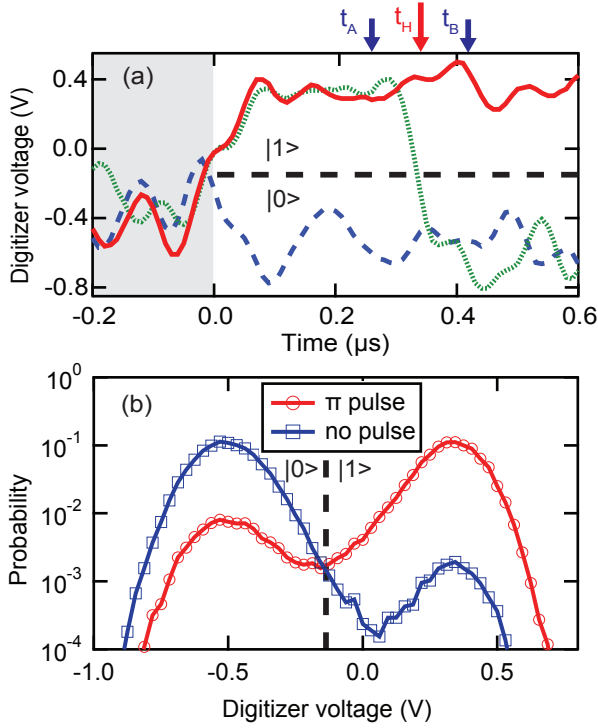


FIG. 2. Qubit readout at $\bar{n} = 14.6$ photons. (Color online) (a) Three individual qubit readouts starting at $t = 0$: excited state (solid red line), ground state (long blue dashes), abrupt quantum jump from the excited to ground state (short green dashes). (b) Log-linear histograms of many ground and excited state preparations, with each histogram bin count normalized to the total number of counts.

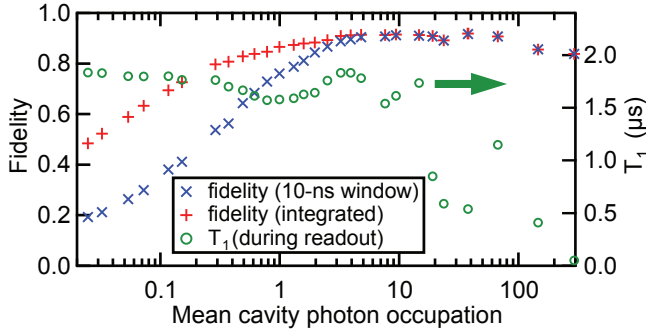


FIG. 3. Raw fidelity and T_1 during readout vs. readout power. (Color online) Fidelity curves measured using a single 10-ns acquisition (blue \times) and using integration (red $+$) merge together when the readout pointer state histograms completely separate. The relaxation time T_1 measured during continuous readout monitoring (green \circ) is referred to the right axis.

exceeds $1.5 \mu\text{s}$; the structure in the data in this regime is likely due to frequency-dependent variation in the electromagnetic environment seen by the qubit as the Larmor frequency is Stark shifted with increasing readout power.

We now examine the measurement histograms in detail to investigate sources of fidelity loss. In particular, we as-

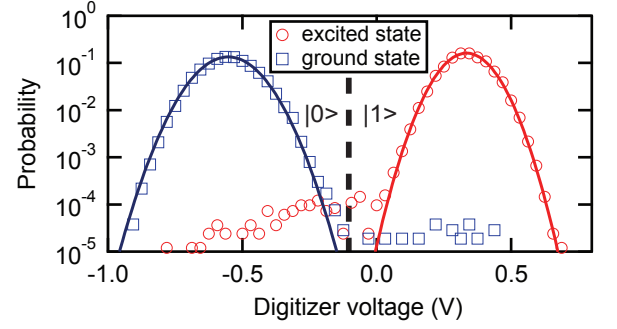


FIG. 4. Pure readout pointer state distributions. (Color online) A two-point correlation procedure is used to exclude qubit transitions and create pure ground and excited state distributions, represented by log-linear histograms, with each histogram bin count normalized to the total number of counts. By totaling the counts on the wrong side of the voltage discrimination threshold, the distributions are determined to be separated to better than one part in 1000.

sess the degree to which the pointer state histograms can be separated. In Fig. 2 (b), we postulated that counts found between the two readout pointer state peaks were due to quantum jumps during measurement. To discard these events and create pure-state distributions, we implement a two-point correlation procedure. The system is probed at times t_A and t_B , as shown in Fig. 2 (a). We retain measurements only when both of these readings return the same value for the qubit state. Thus, the readout exhibiting the abrupt quantum jump is excluded. The 160-ns time difference between these points is several times longer than the response time set by the ~ 10 MHz system bandwidth, thus ensuring minimal autocorrelation between the signals at t_A and t_B , and nearly random distributions at $t = t_H$ (subscript H denotes histogram). The resulting histograms at $t = t_H$ with these outliers removed are shown in Fig. 4 for $\sim 10^5$ ground and excited state readouts. Using the discrimination threshold shown in the figure, we observe only 108 false counts, thus allowing the pointer state histograms to be separated to one part in 1000. Consequently, the finite measurement SNR does not contribute to the observed fidelity loss. This procedure, however, does not correct for those rare events in which the system jumps twice. Unambiguously distinguishing these events is difficult due to the limited system bandwidth, which could be increased in future experiments.

To investigate other sources of fidelity loss, we herald the ground state by inserting a fast measurement pulse prior to qubit manipulation, as shown in the pulse sequence of Fig. 5 (a). With the qubit in thermal equilibrium with the environment, we energize the readout and extract the qubit state at $t = t_S$ (subscript S denotes selection). If the qubit is determined to be in the ground state, no correction is applied; otherwise the subsequent readout is discarded from the total record. Events where

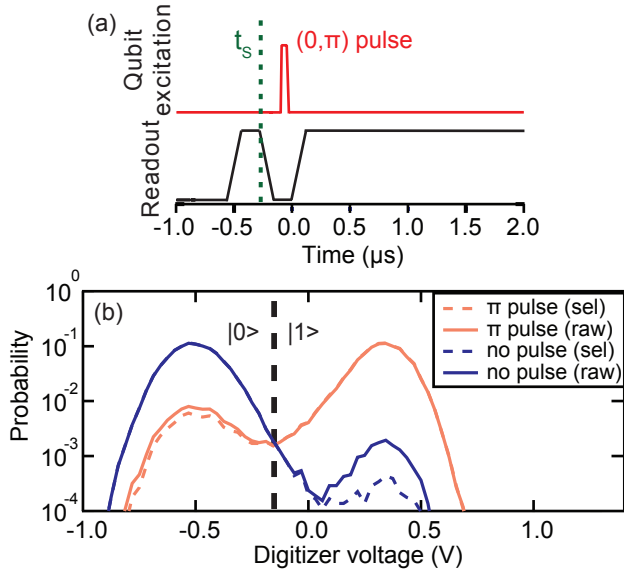


FIG. 5. Heralded state preparation at $\bar{n} = 14.6$. (Color on-line) (a) Pulse sequence used for heralded state preparation. A pure ground state is heralded at $t = t_s$. (b) Log-linear raw readout histograms for $\sim 10^5$ excited and ground state readouts (solid lines) compared with the histograms generated after heralded state preparation (dashed lines). The histogram bin counts are normalized to the total number of counts. An increase in fidelity from 91.0% to 93.9% is reflected in the decreasing size of the smaller peak of the bimodal distributions which are responsible for fidelity loss.

the qubit is spontaneously found in the excited state can be attributed to either remnant thermal population or readout-induced excitation of the ground state [25] during the heralding pulse. With this procedure in place, we again prepare ground and excited state histograms, and observe a fidelity improvement of $2.9 \pm 0.2\%$. We compare the log-linear readout histograms both with (selected) and without (raw) heralded state preparation in Fig. 5 (b). The reduced overlap of the histograms with heralded state preparation is demonstrated by the decreased size of the smaller of the bimodal peaks in both the excited and ground state distributions. This procedure corrects for the remnant thermal population of the excited state.

To separate out the contributions of the remaining sources of fidelity loss, we examine long time traces ($\gg T_1$) with the system prepared in the ground state. We record and analyze the statistics of individual transitions between the qubit states, extracting the average readout induced excitation (Γ_\uparrow) and decay (Γ_\downarrow) rates. The calculated fidelity loss during measurement due to Γ_\uparrow is 0.2%, while the contribution of Γ_\downarrow is negligible. The remaining, unaccounted-for sources of fidelity loss are estimated to contribute 1.5%. We speculate that this loss is explained by errors in excited state preparation, namely π -pulse imperfections and drifts of the Larmor

frequency due to local magnetic flux variations. In Table I, all of the sources of loss and the method by which they are calculated are listed. We note that the dominant loss mechanism is energy relaxation, and calculate its contribution by comparing the readout time and the measured value of T_1 . Currently, there are flux qubits with demonstrated relaxation times on the order of $10 \mu\text{s}$ [5, 26]; in our system, a similar T_1 would reduce the associated fidelity loss to 0.7%. Moreover, one could potentially employ cavities engineered to suppress the spontaneous decay of the qubit [27]. This level of coherence, coupled with heralded ground state preparation, high-precision π pulses [28] and stable magnetic flux, should readily enable readout fidelities in excess of 98% within this low power dispersive measurement architecture.

TABLE I. A budget of fidelity loss at $\bar{n} = 14.6$. The measured fidelity is $91.0 \pm 0.4\%$.

Source of loss	Fidelity loss (%)	Calculation method
T_1 decay	4.4 ± 0.3	measured T_1
thermal population	2.9 ± 0.2	heralding
Γ_\uparrow	0.2 ± 0.1	individual jumps
Γ_\downarrow	0.0 ± 0.2	individual jumps
SNR	< 0.1	pointer state overlap
remaining	1.5	-

Finally, we discuss a fast qubit initialization procedure based on heralding of the ground state. If the excited state is measured during the probe pulse, the state can be immediately reverted with a control pulse and rapidly checked again. This procedure eliminates the need to change the detuning δ [27] to induce Purcell relaxation. The ideal fidelity of this active reset to the ground state is ultimately limited by how the relaxation time of the qubit compares with κ , and is given approximately by the simple formula $F_{\text{reset}} = e^{-2\pi/\kappa T_1} = 93\%$ for our experimental parameters. We measure a reset fidelity of 82%, which is close to the reset fidelity we expect to achieve (84%) after correcting for the fidelity loss ascribed to excited state preparation errors (1.5%) and an extra 140 ns of delay present in the pulse sequence used in this particular experiment (8.1%). The reset procedure could be iterated to achieve enhanced reset fidelity, but for qubits with relaxation times greater than $10 \mu\text{s}$, a single iteration of this procedure would achieve reset with close to 99% fidelity, assuming that the leftover fidelity loss we attribute to imperfect state preparation could be eliminated.

In conclusion, we have demonstrated a fast, analog cQED readout to measure the state of a flux qubit with high single shot fidelity. We use the QND nature of this readout at low powers to demonstrate heralded state preparation. This procedure allows us to obtain a detailed account of the sources of fidelity loss in the read-

out protocol. Moreover, errors due to imperfect ground state initialization can be readily identified and effectively eliminated through post-selection. Extending this further, these errors could be actively corrected in real time if a π pulse were to be triggered based on the outcome of the heralding readout. The dominant remaining source of fidelity loss in our experiment is due to the short energy relaxation time of the qubit. For $T_1 > 10 \mu\text{s}$ with perfect state preparation, we predict a fidelity of greater than 98% in the current readout architecture. We also note that this simple heralding procedure immediately allows for rapid reset of the qubit without the need to change bias parameters. Our readout architecture provides a new tool to study readout-induced backaction in a qubit with a high degree of anharmonicity, complementing previous work on transmon qubits [25, 29].

We thank E. M. Hoskinson and S. Weber for useful discussions and contributions to this project. D.H.S. acknowledges support from a Hertz Foundation Fellowship endowed by Big George Ventures. This work was funded in part by the U.S. Government and by BBN Technologies. Funding is also acknowledged from the ARO under grant W911NF-11-1-0029.

-
- [1] J. Clarke and F. K. Wilhelm, *Nature* **453**, 1031 (2008).
 - [2] M. Neeley, R. C. Bialczak, M. Lenander, E. Lucero, M. Mariantoni, A. D. O’Connell, D. Sank, H. Wang, M. Weides, J. Wenner, Y. Yin, T. Yamamoto, A. N. Cleland, and J. M. Martinis, *Nature* **467**, 570 (2010).
 - [3] L. DiCarlo, M. D. Reed, L. Sun, B. R. Johnson, J. M. Chow, J. M. Gambetta, L. Frunzio, S. M. Girvin, M. H. Devoret, and R. J. Schoelkopf, *Nature* **467**, 574 (2010).
 - [4] I. Siddiqi, *Superconductor Science and Technology* **24**, 091002 (2011).
 - [5] J. Bylander, S. Gustavsson, F. Yan, F. Yoshihara, K. Harrabi, G. Fitch, D. G. Cory, Y. Nakamura, J.-S. Tsai, and W. D. Oliver, *Nature Phys.* **7**, 565 (2011).
 - [6] H. Paik, D. I. Schuster, L. S. Bishop, G. Kirchmair, G. Catelani, A. P. Sears, B. R. Johnson, M. J. Reagor, L. Frunzio, L. I. Glazman, S. M. Girvin, M. H. Devoret, and R. J. Schoelkopf, *Phys. Rev. Lett.* **107**, 240501 (2011).
 - [7] L. DiCarlo, J. M. Chow, J. M. Gambetta, L. S. Bishop, B. R. Johnson, D. I. Schuster, J. Majer, A. Blais, L. Frunzio, S. M. Girvin, M. H. Devoret, and R. J. Schoelkopf, *Nature* **460**, 240 (2009).
 - [8] M. Mariantoni, H. Wang, T. Yamamoto, M. Neeley, R. C. Bialczak, Y. Chen, M. Lenander, E. Lucero, A. D. O’Connell, D. Sank, M. Weides, J. Wenner, Y. Yin, J. Zhao, A. N. Korotkov, A. N. Cleland, and J. M. Martinis, *Science* **334**, 61 (2011).
 - [9] M. D. Reed, L. DiCarlo, B. R. Johnson, L. Sun, D. I. Schuster, L. Frunzio, and R. J. Schoelkopf, *Phys. Rev. Lett.* **105**, 173601 (2010).
 - [10] I. Siddiqi, R. Vijay, M. Metcalfe, E. Boaknin, L. Frunzio, R. J. Schoelkopf, and M. H. Devoret, *Phys. Rev. B* **73**, 054510 (2006).
 - [11] F. Mallet, F. R. Ong, A. Palacios-Laloy, F. Nguyen, P. Bertet, D. Vion, and D. Esteve, *Nature Phys.* **5**, 791 (2009).
 - [12] J. M. Martinis, *Quant. Info. Proc.* **8**, 81 (2009).
 - [13] A. Blais, R.-S. Huang, A. Wallraff, S. M. Girvin, and R. J. Schoelkopf, *Phys. Rev. A* **69**, 062320 (2004).
 - [14] A. Wallraff, D. I. Schuster, A. Blais, L. Frunzio, R.-S. Huang, J. Majer, S. Kumar, S. M. Girvin, and R. J. Schoelkopf, *Nature* **431**, 162 (2004).
 - [15] B. R. Johnson, M. D. Reed, A. A. Houck, D. I. Schuster, L. S. Bishop, E. Ginossar, J. M. Gambetta, L. DiCarlo, L. Frunzio, S. M. Girvin, and R. J. Schoelkopf, *Nature Phys.* **6**, 663 (2010).
 - [16] A. Wallraff, D. I. Schuster, A. Blais, L. Frunzio, J. Majer, M. H. Devoret, S. M. Girvin, and R. J. Schoelkopf, *Phys. Rev. Lett.* **95**, 060501 (2005).
 - [17] R. Vijay, D. H. Slichter, and I. Siddiqi, *Phys. Rev. Lett.* **106**, 110502 (2011).
 - [18] J. E. Johnson, E. M. Hoskinson, C. Macklin, D. H. Slichter, I. Siddiqi, and J. Clarke, *Phys. Rev. B* **84**, 220503 (2011).
 - [19] M. Hatridge, R. Vijay, D. H. Slichter, J. Clarke, and I. Siddiqi, *Phys. Rev. B* **83**, 134501 (2011).
 - [20] N. Piro, F. Rohde, C. Schuck, M. Almendros, J. Huwer, J. Ghosh, A. Haase, M. Hennrich, F. Dubin, and J. Escher, *Nature Phys.* **7**, 17 (2011).
 - [21] A. Palacios-Laloy, F. Mallet, F. Nguyen, F. Ong, P. Bertet, D. Vion, and D. Esteve, *Physica Scripta* **2009**, 014015 (2009).
 - [22] C. H. van der Wal, A. C. J. ter Haar, F. K. Wilhelm, R. N. Schouten, C. J. P. M. Harmans, T. P. Orlando, S. Lloyd, and J. E. Mooij, *Science* **290**, 773 (2000).
 - [23] A. A. Abdumalikov, O. Astafiev, Y. Nakamura, Y. A. Pashkin, and J. S. Tsai, *Phys. Rev. B* **78**, 180502 (2008).
 - [24] J. Gambetta, W. A. Braff, A. Wallraff, S. M. Girvin, and R. J. Schoelkopf, *Phys. Rev. A* **76**, 012325 (2007).
 - [25] M. Boissonneault, J. M. Gambetta, and A. Blais, *Phys. Rev. A* **79**, 013819 (2009).
 - [26] A. D. Córcoles, J. M. Chow, J. M. Gambetta, C. Rigetti, J. R. Rozen, G. A. Keefe, M. B. Rothwell, M. B. Ketchen, and M. Steffen, *Applied Physics Letters* **99**, 181906 (2011).
 - [27] M. D. Reed, B. R. Johnson, A. A. Houck, L. DiCarlo, J. M. Chow, D. I. Schuster, L. Frunzio, and R. J. Schoelkopf, *Applied Physics Letters* **96**, 203110 (2010).
 - [28] J. Bylander, M. S. Rudner, A. V. Shytov, S. O. Valenzuela, D. M. Berns, K. K. Berggren, L. S. Levitov, and W. D. Oliver, *Phys. Rev. B* **80**, 220506 (2009).
 - [29] D. H. Slichter, Ph.D. thesis, University of California, Berkeley (2011).